ADVANCED CERAMIC MATERIALS, 3 [5] 452–56 (1988)

Microstructural Characterization of Commercial Hot-Pressed Boron Nitride

JAMES H. STEELE* and RUTH ENGEL*
Research Center, Armco Inc., Middletown, OH 45043

Microstructural characterization of commercially hot-pressed boron nitride (BN) using SEM and mercury porosimetry are described. Commercial material consists of varying amounts of B_2O_3 (2% to 9%) and fine porosity (2% to 7%) within a bonded three-dimensional network of BN particles. The platelike BN particle morphology, which forms an aggregate by bonding along particle edges, is displayed. A layered structure present within individual BN particles is shown to consist of fine porous layers (<30 nm in thickness), which separate BN regions (100 to 200 nm in thickness) in the plane of the platelets. Size and dispersion of the pores and the continuous B_2O_3 phase are estimated with mercury porosimetry and with SEM after leaching and filling with a liquid bismuth–tin (Bi–Sn) alloy.

The commercial availability of hot-pressed boron nitride (BN) was one of the most important factors in the successful implementation of a horizontal caster for steel. Its lack of wetting by liquid steel, its high thermal conductivity, and its resistance to thermal shock make boron nitride uniquely suited for this application. These properties, and its machinability, allow boron nitride to be made into the refractory component (called a break ring) which couples the tundish to the cooling mold and provides the surface for the start of solidification of the liquid steel. It is thus the most important factor in controlling solidification and surface quality of the steel products. The critical nature of this application has made it imperative to characterize the microstructure as well as the chemistry and physical properties of commercial material. Since very little has been published on the microstructure of hot-pressed BN, this study was undertaken to develop techniques and apply them in characterizing its microstructure. This paper describes the techniques that were developed and presents results from several samples of the hot-pressed material. The observations lead to a description of the volume fractions, the morphologies, and the dispersion of the microstructural constituents, which include the bonded BN particle aggregate, the hygroscopic B_2O_3 phase, and the inherent porosity.

LITERATURE REVIEW

Boron nitride has been known for many years to possess attractive refractory, electrical, thermal, and lubricating properties; however, difficulty in fabricating it into a dense body has limited its applications. The modern hot-pressing technology is based on the work of Taylor,[1] in which BN powder is pressed in graphite dies at relatively high temperatures and moderate pressures. BN powder can be formed by a number of chemical reactions such as

$$B_2O_3 + 2NH_3 \longrightarrow 2BN + 3H_2O \quad (1)$$

which provides a cheap and convenient production method. The powder contains small amounts of B_2O_3, which allows it to be hot-pressed at temperatures as low as 900°C and which is necessary for the formation of a dense body with reasonable room-temperature strength. This property is probably the result of liquid phase sintering, since B_2O_3 is known to form a liquid above 500°C.[2] However, the presence of B_2O_3 in the final hot-pressed material may cause problems in this application since B_2O_3 is highly hygroscopic.

BN was shown by Pease[3] to exhibit a simple hexagonal crystal structure with nearly flat hexagonal BN rings stacked directly over each other, as illustrated in Fig. 1. He also proposed that individual BN particles contained a layered structure formed by platelike crystallites parallel to the basal plane. This structure was proposed to explain the broadening of XRD peaks from different sets of crystallographic planes. The layered structure envisaged by Pease[3] for particles recrystallized for 2 h at 2030°C is shown in Fig. 2 along with the proposed dimensions. He also suggested that the layered crystallites might be the result of faults parallel to the basal plane similar to those observed in graphite. A more recent study on hot-pressed material has also suggested a crystallite size of ≈40 nm from X-ray broadening.[4] Direct observations of BN particles, their crystallite size, or their layered structure have not been reported in the literature.

Chemical analyses on a number of commercial break rings have shown that significant variability occurs in their B_2O_3 content.[5] The range of this variability was 2% to 9.5% by weight as measured by soluble borate content. In addition, small amounts (0.2 to 0.3 wt%) of silica, alumina, and alkaline-earth oxides have been reported in hot-pressed material.[4] The presence of hygroscopic B_2O_3 causes considerable difficulty with regard to storage, density measurement, and sample preparation for microstructural examination. This difficulty with hygroscopic effects is illustrated by data (shown in Fig. 3) that suggest a correlation between apparent porosity and B_2O_3 content. These measurements of porosity were obtained using the ASTM method for apparent density in water and thus may involve dissolution of B_2O_3. Significant variability has also been observed in the strength properties at ambient temperature. These results are shown in Figs. 4 and 5, where modulus of rupture is plotted as a function of B_2O_3 content and apparent porosity. These trends indicate that the presence of B_2O_3 leads to an increase in room-temperature strength, whereas the presence of porosity tends to decrease it, and that both variables exhibit a wide range of variability. Thus, it is extremely important to be able to characterize the amount and dispersion of the B_2O_3 and the inherent porosity present in the hot-pressed material.

EXPERIMENTAL PROCEDURE

The samples were selected from commercial break rings that had been rejected because of improper size or machining. Chemical analysis of the B_2O_3 content was obtained from the amount of soluble borates present. The solubility of B_2O_3 in both water and alcohol caused considerable difficulty in retaining this phase during preparation for microscopic examination. The ability to leach out the B_2O_3 was used to obtain indirect evidence of its amount, size, and dispersion through mercury intrusion and pressure im-

*Member, the American Ceramic Society.
*Now at Los Alamos National Lab, Los Alamos, NM.
†Porous Materials, Inc., Ithaca, NY.

Manuscript No. 199976. Received June 10, 1987; approved January 22, 1988.
Presented at the 88th Annual Meeting of the American Ceramic Society, Chicago, IL, April 29, 1986 (Joint Session III, Paper No. 8–JIII–86).

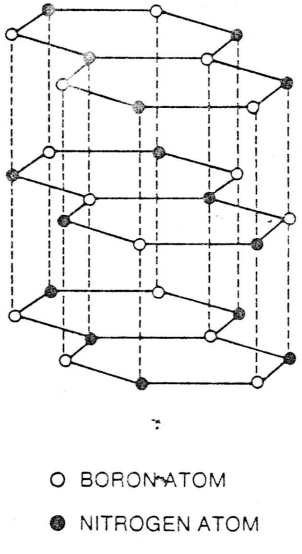

Fig. 1. Crystal structure of hexagonal BN (Ref. 3).

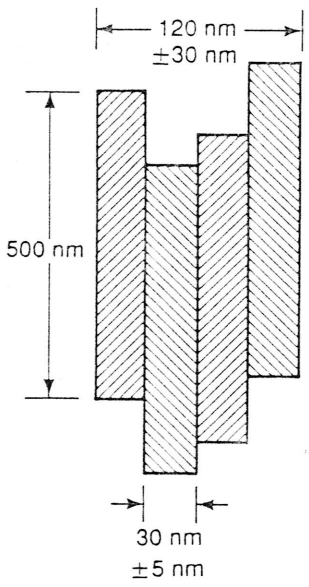

Fig. 2. Schematic illustration of the layered BN particle microstructure as suggested by Pease.[3]

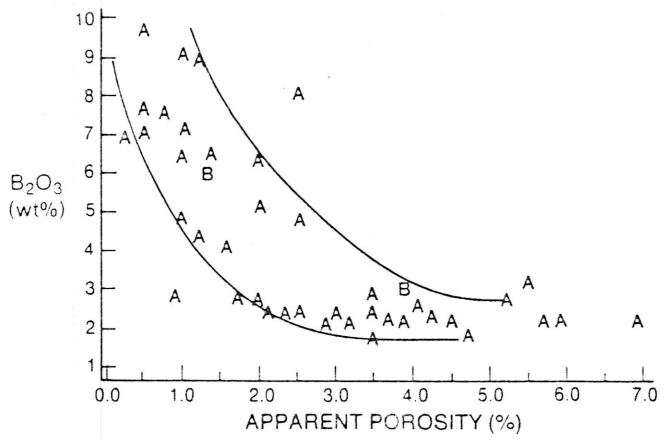

Fig. 3. Soluble B_2O_3 content as a function of apparent porosity (A = one observation and B = two observations).

pregnation of a low-melting-point bismuth–tin (Bi–Sn) alloy.

XRD patterns obtained on several samples showed primarily lines from the hexagonal BN structure with some weaker diffraction peaks from crystalline B_2O_3. The X-ray results also indicated that the BN crystallites were not highly textured nor were they small enough to produce significant crystallite size (or Scherrer) broadening. Thus, the crystallite size appears to be somewhat larger than the 40 nm reported by Simpson and Stuckes[4] for hot-pressed material.

Samples were prepared for examination by scanning electron microscopy (SEM) by dry-cutting with a diamond saw to minimize dissolution of the B_2O_3 phase. Sections both parallel and perpendicular to the direction of hot-pressing were prepared in an effort to observe and characterize microstructural anisotropy. They were then mounted in a low-melting-point Bi–Sn alloy, which was allowed to solidify under a pressure of 35 MPa (5000 psi). This caused the porosity formed by leaching of the B_2O_3 to be filled with the liquid metal for all open pores with sizes >30 nm. Mounted samples were prepared by standard methods of rough and fine grinding using water as a lubricant.

Final polishing was conducted using diamond abrasives with a water-soluble oil-base extender. Since no direct attempt was made to use fluids which would not dissolve B_2O_3, all of the polished sections observed had been leached of the B_2O_3 phase. After the sections were polished, the cross sections were argon-ion etched using a commercial system which was cryopumped to obtain clean vacuum conditions. The samples were examined in polarized light with an optical microscope and in the SEM using both secondary and backscatter detectors for imaging. A difference in microstructure with section orientation could not be detected, even though it was expected since the strength was somewhat different parallel and perpendicular to the direction of hot-pressing.

Mercury porosimetry data were obtained using a commercial computer-controlled system on two samples from the same break ring that had been sectioned for microscopy.[†] The sample pieces were dry-cut into slices several millimeters thick. Pressure–penetration curves were obtained on the samples in the as-cut condition and after leaching for 3 h in methanol. The maximum pressure used was 207 MPa (30 000 psi), which corresponds to the pressure necessary to fill a cylindrical capillary 6 nm in diameter, assuming a contact angle of 130° between Hg and BN. Relative density data before and after leaching were also obtained.

RESULTS AND DISCUSSION

MERCURY POROSIMETRY

The results from mercury porosimetry are shown in Fig. 6 as pressure–penetration curves for two samples from a break ring containing 7.3 wt% (i.e., 8.7 vol%) B_2O_3, as determined by

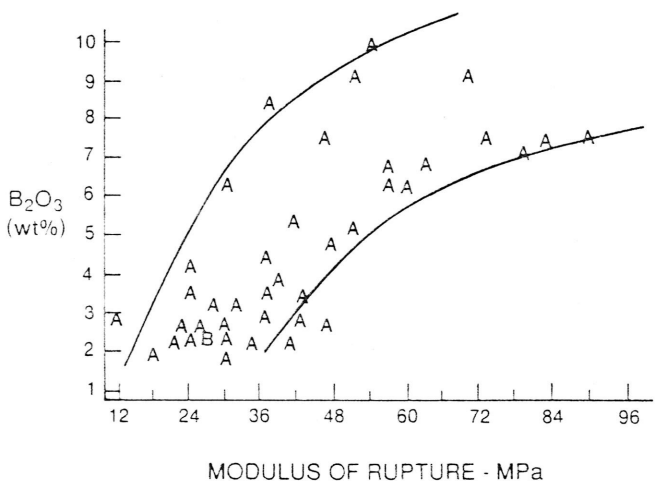

Fig. 4. Room-temperature modulus-of-rupture as a function of soluble B_2O_3 content (A = one observation and B = two observations).

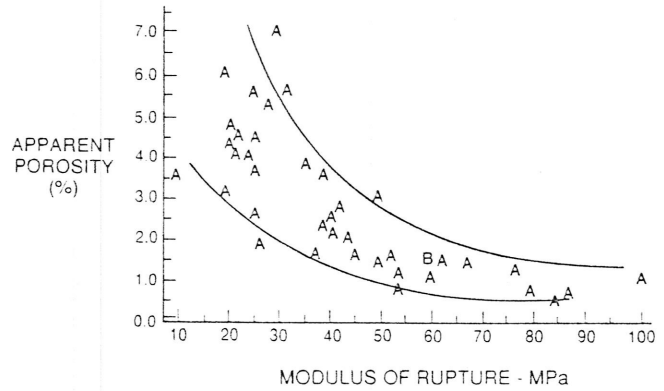

Fig. 5. Room-temperature modulus-of-rupture as a function of apparent porosity (A = one observation and B = two observations).

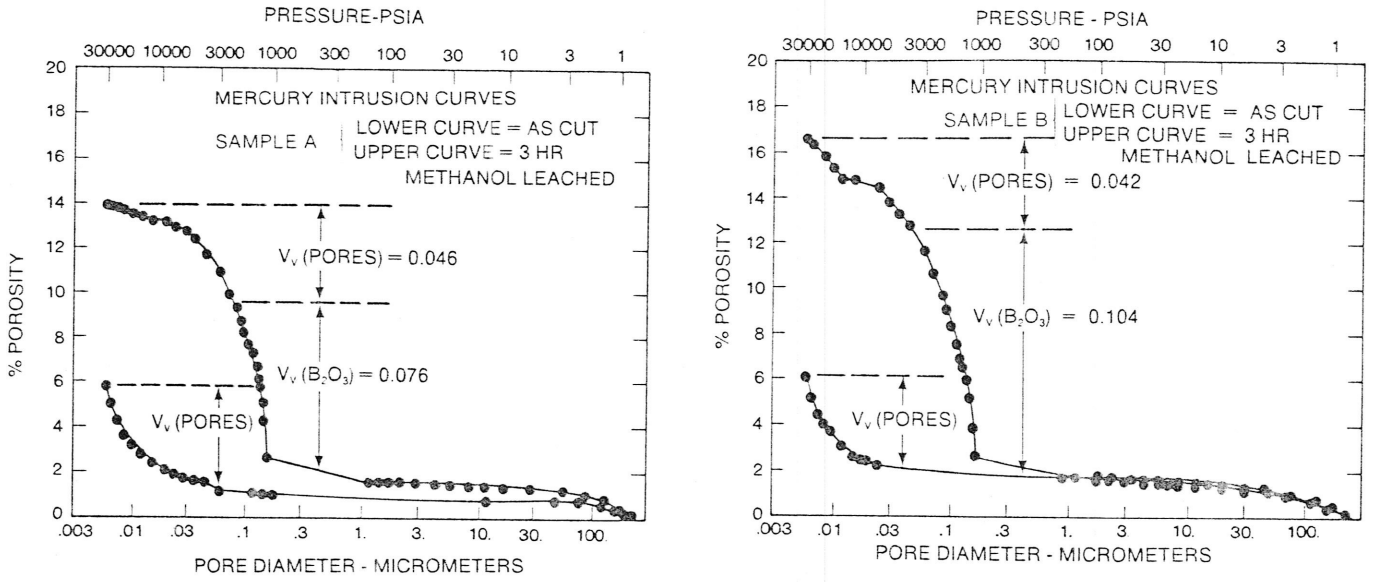

Fig. 6. Mercury intrusion curves of samples A and B showing the effect of methanol leaching of the soluble B_2O_3 phase. Estimates of volume fraction (V_v) of porosity and the leached B_2O_3 phase are given.

chemical analyses. Penetration curves are presented for dry-cut adjacent pieces before and after leaching in methanol. The estimated volume fractions of inherent open porosity are marked on the figures. Volume fraction estimates of the porosity formed by leaching the B_2O_3 phase were obtained by subtracting the amounts of porosity measured before and after leaching. Note that there appears to be a significant difference in the volume fraction of B_2O_3 between samples taken from the same break ring. It is not clear, however, whether this difference is the result of experimental error in the subtraction method or actual chemical heterogeneity between the original break ring samples. The intrusion curves show that the size of the inherent porosity is <30 nm and that the size of the porosity formed by removal of the B_2O_3 phase is between 30 and 200 nm. Although this size is somewhat smaller than observed using the SEM on cross sections, it is consistent with the current interpretation[6] that the mercury intrusion process exhibits a percolation threshold phenomenon which tends to bias calculated pore sizes toward smaller values. Apparent density values and the volume fractions of inherent porosity estimated from the four mercury-intruded samples are listed in Table I with estimates of the solid densities obtained from these two values. Note that the value of 2.36 is higher than the theoretical density of 2.27 for hexagonal BN. This difference may be caused by surface effects which control the initial 1% to 2% apparent mercury penetration for sizes >1 μm.[7] Corrected values for solid density which account for this surface effect are shown in parentheses. The corrected value of 2.31 for the methanol-leached B sample appears to be within experimental error of the theoretical density of BN. Volume fraction estimates for the B_2O_3 phase obtained from bulk chemical analysis and from the mercury-intrusion curves were used to calculate the volume fraction of BN. It can be observed from the last column in Table I that the calculated volume fraction values obtained by the two methods are very consistent with an average value of ≈0.87 (i.e., 87 vol%) BN.

MICROSTRUCTURAL OBSERVATIONS

The hot-pressed BN microstructure is illustrated by the polarized light micrograph shown in Fig. 7. Argon-ion etching removes the flowed surface layer left after diamond polishing and allows the reflectivity differences between individual BN particles to be observed. The lighter regions, which are ≈10 μm in size and have higher reflectivity, appear to be sections through platelike BN particles, which are oriented parallel to the sectioning plane. It is thus likely that these sections tend to be parallel to the basal plane of the hexagonal BN. This interpretation would explain the reflectivity differences observed under polarized light since the hexagonal BN is similar to graphite with regard to optical anisotropy.[8] It also suggests that the particle morphologies may represent individual crystallites with the basal plane oriented parallel to the larger dimension of the plate.

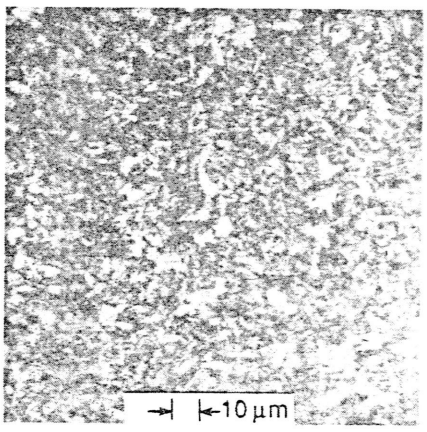

Fig. 7. Polarized-light micrograph from a mechanically polished and argon-ion-etched sample showing optical anisotropy of the BN particles.

Table I. Mercury Porosimetry Data

	Apparent density (g/cm³)	Volume fraction open (porosity)*	Solid density (g/cm³)	Estimated volume fraction B_2O_3	Calculated volume fraction BN†
As-cut sample A	1.95	0.058 (0.046)	2.07 (2.04)	0.087‡	0.867
Methanol leached A	1.92	0.139 (0.122)	2.23 (2.19)	0.076§	0.878
As-cut sample B	2.00	0.061 (0.042)	2.13 (2.09)	0.087‡	0.871
Methanol leached B	1.97	0.165 (0.146)	2.36 (2.31)	0.104§	0.854

*Numbers in parentheses indicate volume fraction (V_v) of open pores <1 μm. †Calculated from rule of mixtures, $V_v(B_2O_3) + V_v(BN) + V_v(\text{porosity}) = 1$. ‡Volume fraction of soluble B_2O_3 from chemical analysis of 7.3 wt%. §Estimated from the difference between the as-cut and leached samples using the porosity values <1 μm.

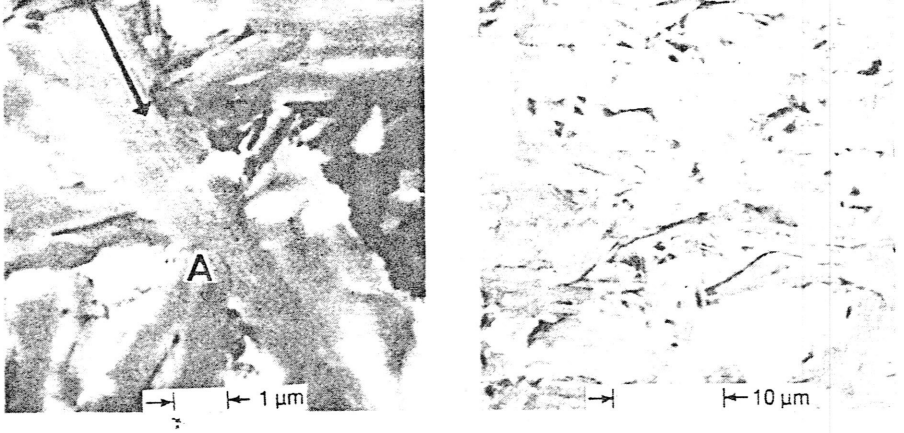

Fig. 8. Backscatter electron micrographs from a mechanically polished and argon-ion-etched sample illustrating the platelike particle morphology, the thin porous layers, bonding at particle edges, e.g., at region A, and fine porosity forming layered BN structure (arrow). Gray areas are BN particles and black areas are pores where B_2O_3 was leached from surface.

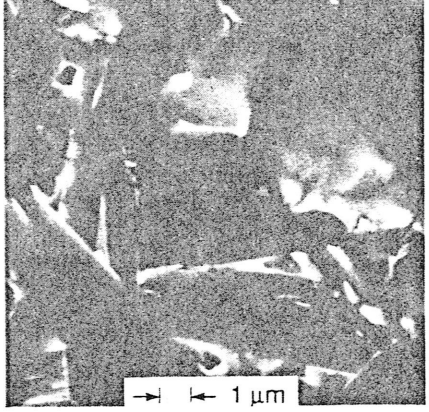

Fig. 9. Secondary electron micrograph from a mechanically polished sample showing Bi–Sn filled porosity formed by methanol leaching of the B_2O_3 phase.

Finer details of the BN particle microstructure are shown by the backscatter electron micrographs presented in Fig. 8. Careful examination reveals that the platelike particles tend to be joined or bonded along their edges. This behavior is indicated by continuity of the backscatter contrast as observed at the particle edges in the region marked A. This observation implies that the BN particles tend to form a three-dimensional aggregate by bonding along ends of their basal planes. This result would not be surprising since the hexagonal structure contains only one type of strong bond, the covalent BN bond joining each atom to its three coplanar nearest neighbors, as indicated in Fig. 1. The larger dark regions, which are areas with very low backscatter intensity, are caused by porosity. As indicated previously, these larger pores are the result of leaching of the B_2O_3 phase during polishing. This porosity, which represents the B_2O_3-phase regions, forms a continuous network within the interstices of the BN particle aggregate. The dark lines parallel to larger dimension of the particles are caused by extremely fine layers of porosity within the BN particles. Note that these interpretations are consistent with the mercury intrusion results.

The coarse porosity is more readily observed after impregnation with the liquid Bi–Sn alloy as shown by the secondary electron micrograph presented in Fig. 9. The diffuse shading of the bright areas, which are associated with the high atomic number Bi–Sn alloy, is a result of relative transparency of the BN matrix to higher energy backscatter electrons. This behavior allows the filled porosity to be observed below the polished surface. Stereo pairs were used to verify this interpretation, which implies that the bright features represent projected images of thin platelike regions between the BN particles. The thickness of the filled pores is thus estimated by the widths of the thin bright lines where the platelets are oriented normal to the sectioning plane. On this basis, the thickness of the porosity is estimated as 0.1 to 0.3 μm, which is consistent with the mercury-intrusion results, as indicated previously. High-contrast backscatter images, which are presented in Fig. 10, display similar effects. These projected images, which involve an estimated depth of ≈ 2 μm, cause the apparent area fraction for B_2O_3 to be larger than the 8.7% expected from a two-dimensional section.[9]

A schematic drawing elucidating the proposed microstructure and the projected image interpretation for the hot-pressed composite material is presented in Fig. 11. This description provides a consistent explanation for the results of this study, as well as those of Pease[3] and Simpson and Stuckes.[4]

CONCLUSIONS

The techniques of mercury intrusion and scanning electron microscopy provide a unique and very powerful combination of analytical tools for characterizing the microstructure of the hot-pressed BN material. Argon-ion etching is shown to provide an excellent method for removing the flowed layers produced by mechanical polishing to reveal the BN particles and their bonded microstructure. A consistent set of interpretations of the observed BN particle and aggregate microstructure within the hot-pressed material are summarized by the schematic drawing shown in

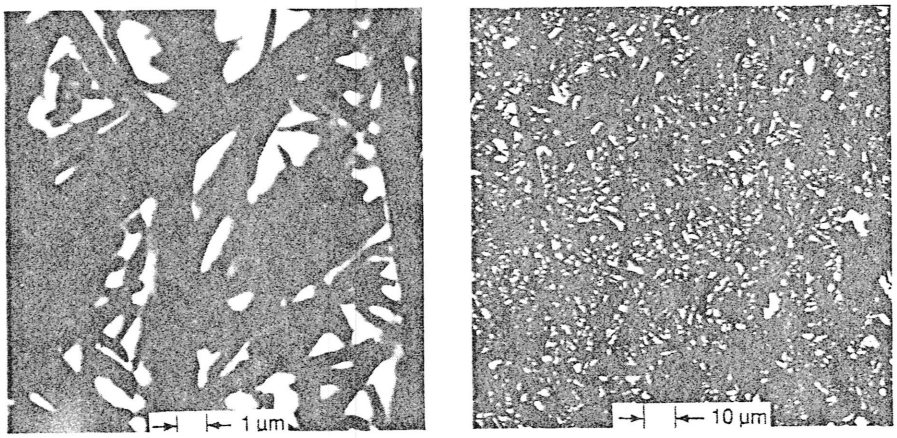

Fig. 10. Backscatter electron micrographs from the sample shown in Fig. 9.

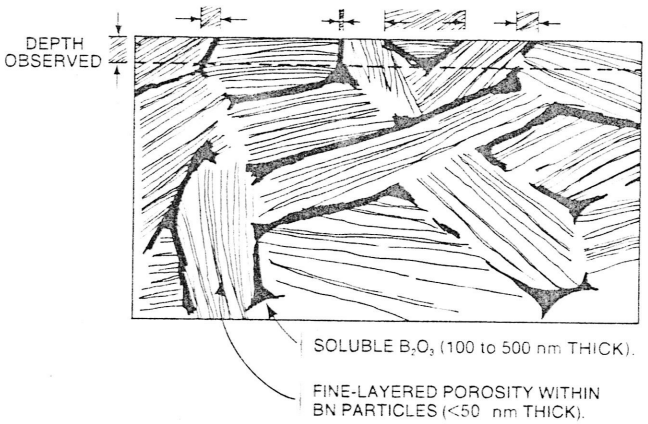

Fig. 11. Sketch illustrating the microstructural observations on the hot-pressed BN composite material. Arrows mark projected widths observed from Bi–Sn-filled pores.

Fig. 11. A continuous three-dimensional aggregate of BN particles with a platelike morphology and sizes of ≈1 to 10 μm is shown to be formed by bonding along particle edges. Mercury intrusion and impregnation of the porosity formed by leaching of the B_2O_3 phase with liquid Bi–Sn were applied to show that the interstices of the BN aggregate are filled by a thin continuous network of B_2O_3 with a thickness of 100 to 300 nm. The individual BN particles are observed to contain layers of very fine porosity (<30 nm thick), which are speculated to be parallel to the basal plane of the hexagonal crystallites. Significant anisotropy in the particle orientation with the direction of hot-pressing was not observed.

ACKNOWLEDGMENT

The authors thank Chris Muller for her assistance in sample preparation and examination with the SEM.

REFERENCES

[1]K. M. Taylor, "Hot-Pressed Boron Nitride," *Ind. Eng. Chem.*, **47** [12] 2506–509 (1955).
[2]M. J. Aziz, E. Nygren, J. F. Hays, and D. Turnbull, "Crystal Growth Kinetics of Boron Oxide Under Pressure," *J. Appl. Phys.*, **57** [6] 2233–42 (1985).
[3]R. S. Pease, "An X-ray Study of Boron Nitride," *Acta Crystallogr.*, **5**, 356–61 (1952).
[4]A. Simpson and A. D. Stuckes, "The Thermal Conductivity of 'Isotropic' and Hot-Pressed Boron Nitride," *J. Phys. D*, **9**, 621–30 (1976).
[5]R. Engel, "Laboratory Testing of Boron Nitride Break Rings"; pp. 329–39 in Proceedings of the 43rd Electric Furnace Conference, 1985.
[6]F. A. L. Dullien, "Woods Metal Porosimetry and its Relation to Mercury Porosimetry," *Powder Technol.*, **29**, 109–16 (1981).
[7]A. J. Katz and A. H. Thompson, "Quantitative Prediction of Permeability in Porous Rock," *Phys. Rev. B*, **34** [11] 8179–81 (1986).
[8]W. E. Tröger, "Optical Determination of Rock-Forming Minerals"; p. 16 in Schweizerbartische Verlagsbuchhandlung, 1971.
[9]E. E. Underwood, Quantitative Stereology, Addison-Wesley, 1970; p. 160. □